Processing the Teal South 4C-4D seismic survey

Carlos Rodriguez-Suarez, Robert R. Stewart and Han-Xing Lu

ABSTRACT

Repeated 4C-3D seismic surveys have been acquired over the Teal South field, Gulf of Mexico. This paper reports the processing of the second 4C-3D data set, acquired in the spring of 1999.

Conventional processing of P-P and P-S data (including asymptotic binning for horizontal components) and CREWES specific flows were applied to the data. The best quality sections were realized from the hydrophone measurements, followed by the vertical component and then the radial component. The use of depth-variant stacks and anisotropic stacks in the radial component did not present improved results at this point.

3-D pre-stack time migration generated low-frequency sections on vertical and hydrophone data but better quality on radial component. No P-wave energy was found in the radial component, but there is evidence of vertical component contamination with converted-wave energy. Separation of these modes into their components and use of different V_P/V_S ratios for asymptotic binning are future work priorities.

From the three methods used investigate receiver coupling of the cable to the ocean floor (trenched, sand-bagged, lain), the best results were found with cable laid on the sea bottom and receivers taped to it.

INTRODUCTION

The Teal South 4C-4D seismic project is an initiative to investigate the use of multicomponent seismic data in assisting the monitoring of reservoir fluid movements. The project is being coordinated by the Energy Research Clearing House (ERCH) and Texaco – the operators of the Teal South field, on Eugene Island Block 354, in the Gulf of Mexico (Figure 1). Texaco acquired a first 4C-3D in July 1997, using four ocean bottom cables (OBC). This report summarizes the acquisition and presents some processing results for the second 4C-3D, acquired in April 1999.

Teal South was selected by ERCH because: 1) it was thought that oil production over a time interval as short as four months could create petrophysical changes in the reservoirs strong enough to be detected by surface seismic data; 2) Texaco had already done some time-lapse study in the area, using streamer acquisition, and 3) the relatively small area of the reservoirs. The water depth in the area is approximately constant and around 85 m.

For the first 3-D survey, Roche et al. (1999) report that receiver locations were determined precisely by the use of acoustic transponders, but orientation is only

approximated. The apparent receiver orientation was obtained using P-wave first arrivals. Some uncertainties observed are attributed by the authors to both computational errors (caused by shallow sediments anisotropy) and physical process (the receiver dual axis gimbals and/or the transducer coupling may have different azimuth sensitivity).

On the same data, Purnell et al. (1999) used 3-D phase-shift plus interpolation (PSPI) depth migration on common-receiver gathers. Before migration, offset-dependent wavefront spreading correction, Q compensation and surface-consistence methods (amplitude compensation, predictive deconvolution, and residual statics) were applied in the data. Comparing the result of this processing with a conventional CMP stack followed by 3-D poststack time migration, they concluded that, for a structural analyses at Teal South, the later sequence produces results sufficiently good.

Figure 1 – Location of theTeal South field in the Gulf of Mexico (from Ebrom *et al.*, 1998).

ACQUISITION

Figure 2 shows the shot point and receiver position. Most information in this section comes from a report by Baker Hughes/Western Geophysical (1999).

Seven cables were used in a fixed configuration. Four cables, each cable with 6 receivers spaced 200 m, were laid along the E-W direction; the distance between cables was 400 m – this is a receiver pattern close to the one used on the first 3-D. Three additional cables (each cable having 4 receivers spaced at 400 m) were laid in a N-S direction, spaced 100 m apart. The whole cable deployment took five days, in February 1999.

As one objective for the Teal South project is to analyze how different ways of cable laying to the sea floor produces different response, 5 cables were buried

(trenched) 1 m under the sea floor, 1 cable laid on sea floor and had the receivers taped to it and another one laid on sea floor, and had the receivers taped and sandbagged. A remote operated vehicle (ROV) was used on cable trenching. The trenched cables are the ones oriented E-W and the westernmost along N-S. The easternmost N-S cable is the one with bags of sand put over the receiver units, and the N-S cable at the middle is the one with the receivers taped to the cable.

The shot point grid was 25 x 25 m, over an area of approximately 4 x 3 km^2. In total, there are around 19,200 shots. The data were stored in tapes, located in four different buoys spread in the area. These tapes could record 10 hours of shooting. The shooting, in an N-S direction, went from April 12 to 26, using a Western Geophysical boat. Western also supplied navigation (DGPS) and support; I/O supplied the recording instruments, DigiCourse the equipment for receiver location and buoys for cable retrieval and Oceaneering the ROV for cable trenching.

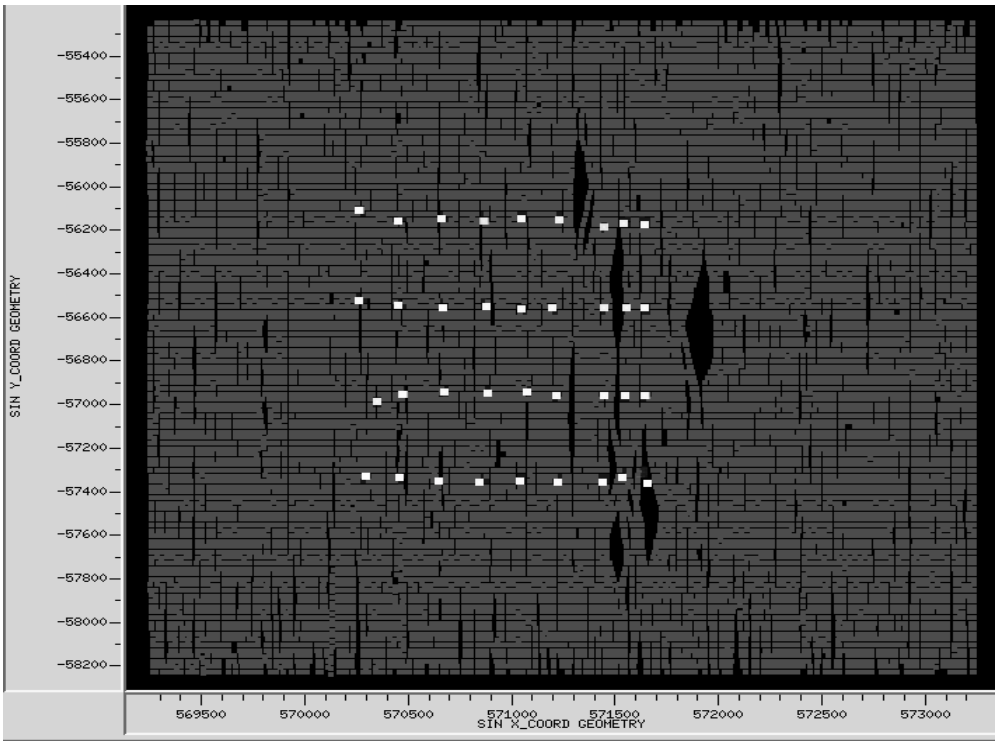

Figure 2 – Shot point (gray) and receiver (white) position. Observe shot gaps, 4 receivers cables along E-W (with 6 units) and 3 cables along N-S (4 units). E-W cables and westernmost N-S cable were trenched, middle N-S cable was laid on sea-bottom and had receivers taped to the cable and easternmost N-S cable was laid on sea-bottom and had receivers taped and sandbagged.

Additional information on the acquisition parameters is presented in Appendix I.

PRE-PROCESSING AND QUALITY CONTROL

The data were resampled to 4 ms (from the original 2 ms) for all components to save disk space and make the processing faster. The maximum recording was changed to 4.5 s for the vertical and hydrophone components and to 6.0 s for the

horizontal (radial and transverse) components. The trace header information was converted from feet to meters.

A land configuration was used for the geometry. The CDP fold distribution for all components, when a 25 m bin size is used, is shown on Figure 3. For the horizontal components, the fold distribution is obtained after asymptotic binning using a V_P/V_S ratio of 2.0. As expected from the high number of shots, a high and homogenous fold is present for vertical and hydrophone. For the horizontal components, the maximum fold valued more than double, but the distribution is more heterogeneous and a smaller area is imaged.

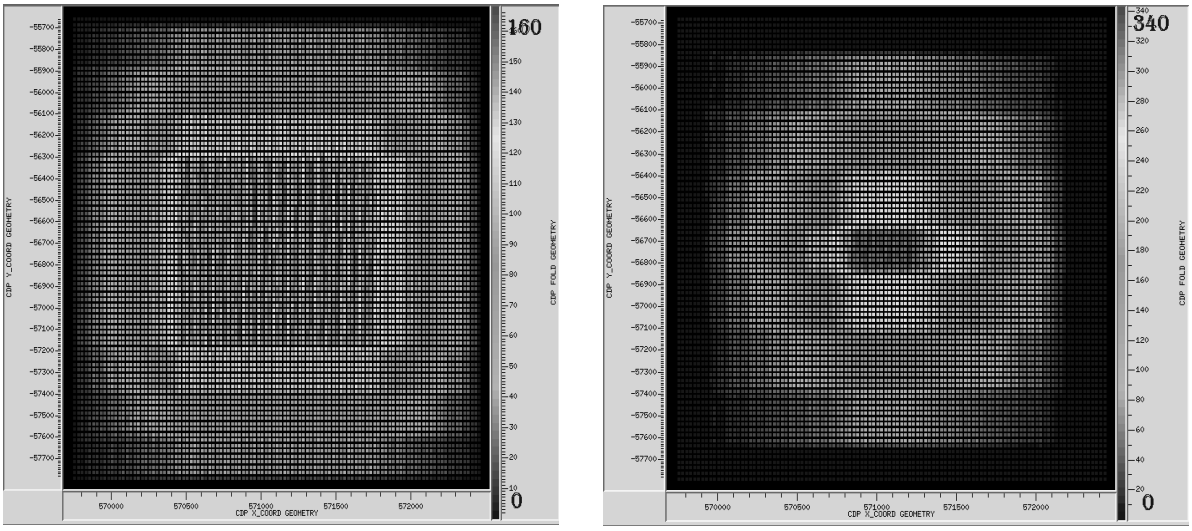

Figure 3 – CDP fold for vertical and hydrophone (left) and radial and transverse after asymptotic binning using Vp/Vs of 2.0 (right).

To use the concepts of 'radial' and 'transverse', the original horizontal components have to be rotated to a new set of orthogonal axis. The radial direction of the new axis is given by the source-receiver azimuth and the transverse by the orthogonal to this direction. Figure 4 shows an example for a reorientation performed on a source-receiver pair. One can see that the source-receiver energy alignment is very good. We could not find in the literature if this is the case for most offshore surveys, but from our experience, we know this may not be true for land 3-D multicomponent. The energy alignment was performed using a time window of approximately 500 ms, centered in the first break (in general, the direct wave).

Another issue for horizontal component processing is to obtain the correct polarity. For 2-D, the polarity correction is obtained simply by reversing the polarity for symmetric offsets (either positive or negative). On 3-D the polarity reversal may be more difficult, and should be performed simultaneously to the reorientation. Figure 5 shows that ProMAX reorientation also takes care of the necessary polarity correction, by considering the amplitude sign of the signal, and not only its energy or absolute amplitude value.

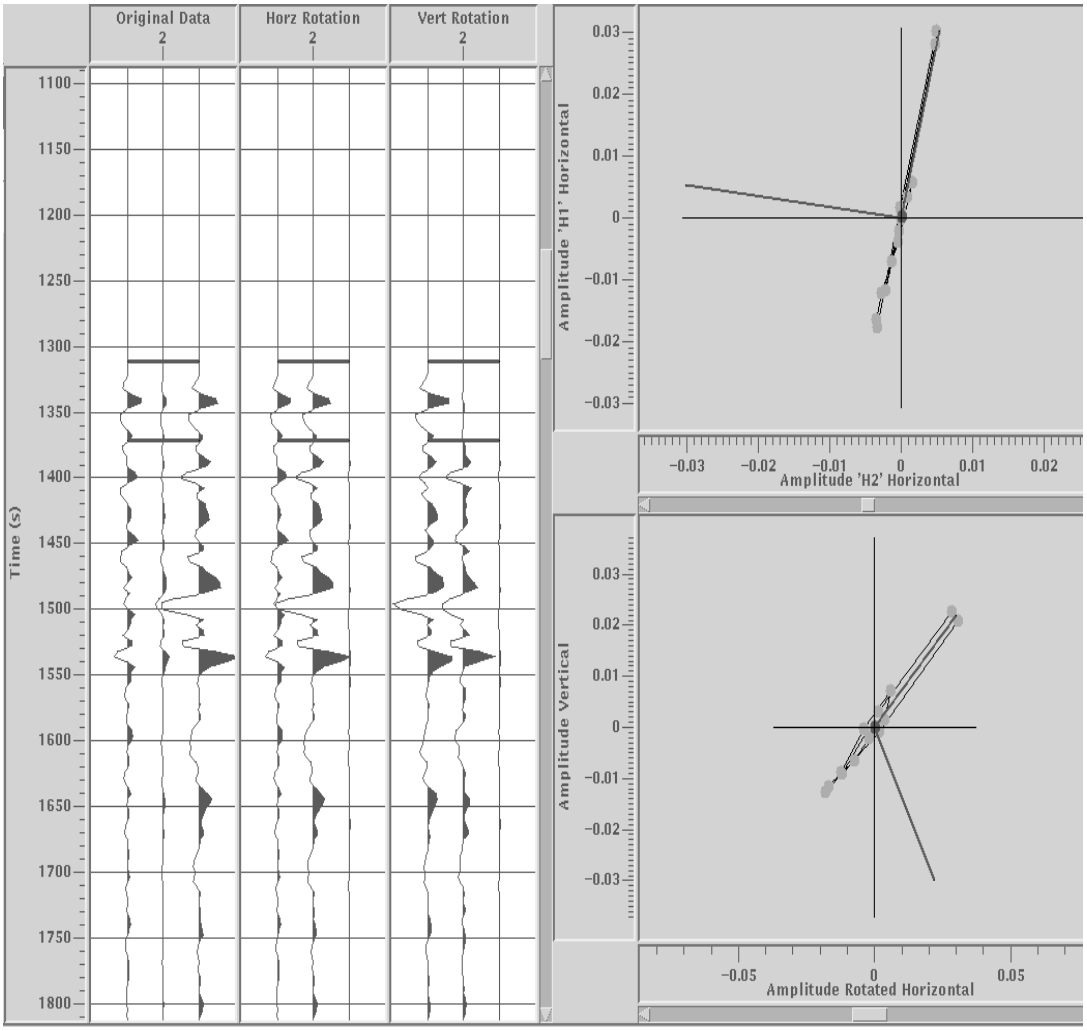

Figure 4 – Reorientation of horizontal components. On left the input (original) data from a specific source-receiver pair (from left, vertical, radial and transverse components). In the middle, the three components after horizontal rotation: most horizontal energy is aligned in the source-receiver direction (trace 2). At right the traces after vertical rotation (not used in this processing). The thick lines from around 1310 to 1370 ms shows the time window used for the energy alignment. Top right shows the original (acquisition) orientation on thin axis and the energy alignment along the new direction (dots and thick axis). The new radial component is defined by this energy alignment, the new transverse by its orthogonal. Bottom left is as top right, but for a (new) radial and vertical hodogram (vertical rotation was NOT used in this processing).

First break energy was canceled by a time and space variant top mute. The source depth was moved to the sea bottom using a time shift, so that the sea bottom was the new datum and the water layer was removed from the processing.

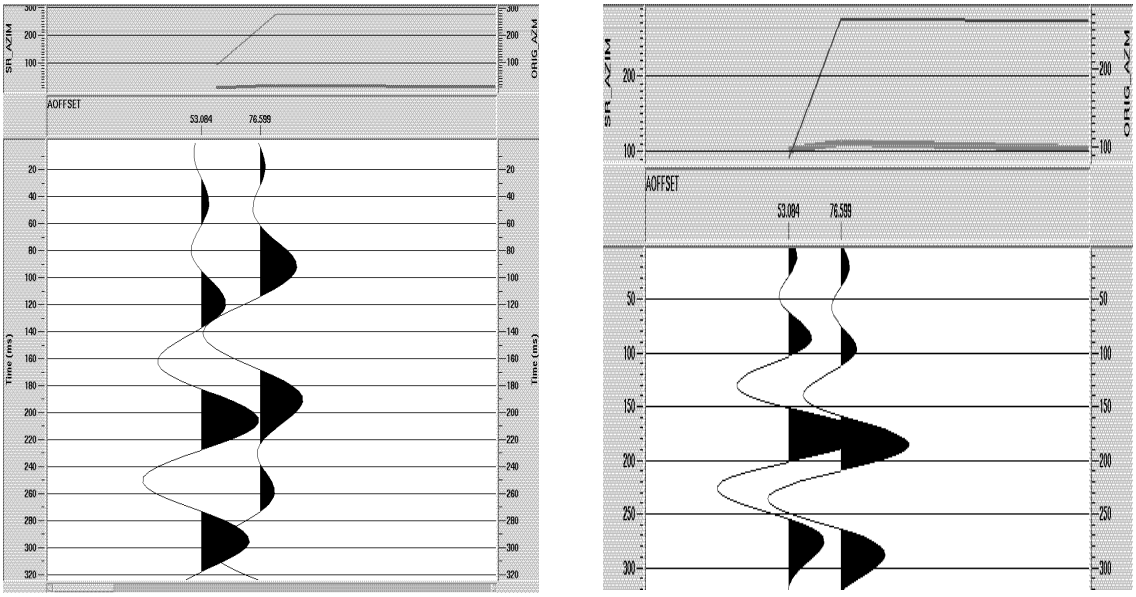

Figure 5 – Comparison of two traces before (left) and after (right) reorientation. Both traces are related to the same shot point, the left trace for a receiver located west of the shot (negative offset), the trace at right at east of the shot point (positive offset). The thick line at the top shows the original component azimuth (close to 90^0); the thin line the new (source-receiver) azimuth after reorientation. Observe that in the left trace the azimuth is not changed, while for the trace at right an 180^0 phase change occurs. The apparent phase difference is due to different travel time plus different static correction (not applied).

A comparison between the average trace energy for all components (after horizontal reorientation is performed), shown in Figure 6, is a good quality control tool. This process is good also to find which maximum amplitude value should be allowed for each component, so that noise (spike) traces can be zeroed. Vertical and radial have the best energy distribution among traces. The hydrophone data may be expected to be somewhat noisy, as there is a strong variation in energy content for adjacent traces. This noise may be to the inherent higher susceptibility (compared to geophones) of this type of receiver to energy trapped in the water layer as reverberation. We also see that: 1) the vertical has a lower energy content (mode around 0.001) than all other components (mode around 0.002), and 2) the horizontal components have much higher maximum values (0.065 for radial and 0.145 for transverse) than vertical (0.026) and hydrophone (0.03). Although these higher values are related probably to more noise traces in the data, no reason other than receiver susceptibility could be found for them to occur more in the horizontal components.

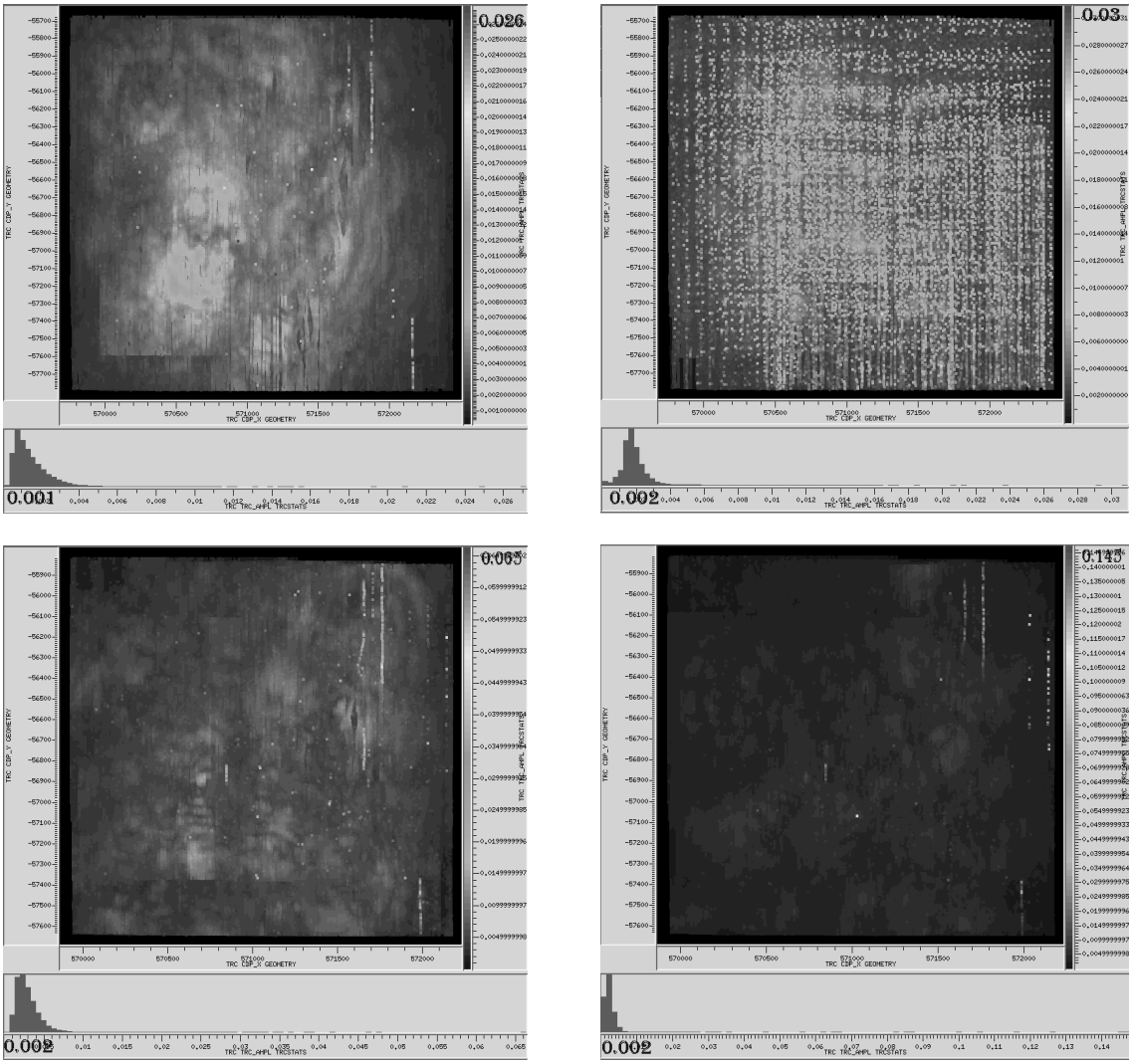

Figure 6 – Average energy per trace for vertical (top left), hydrophone (top right), radial (bottom left) and transverse (bottom right) components.

After top mute and moving the source datum to sea bottom, noisy traces were killed, using a maximum amplitude value obtained from the average trace energy. Then amplitude recovery was performed, assuming a spherical divergence correction according to a $1/tV^2$ equation, where t is travel time and V RMS velocity (considered equal to NMO correction velocity). For all components except the vertical, a correction for inelastic effects was also applied, using an attenuation factor (α) of 0.002.

The dominant frequency is another interesting parameter to be compared between the components and analyzed for each individual component. This is shown in Figure 7. The hydrophone has the highest dominant frequency (around 40 Hz), but it may be related to more high frequency noise (energy reverberation in the water) than to a high frequency content in the signal amplitude spectrum. The horizontal components have almost the same dominant frequency, what is expected. One could expect a higher frequency in the vertical component, as the value is close to the horizontal

components. A reason for this (possible) lower frequency content and also for it to be close to the horizontal components is a contamination of shear-wave (converted) energy in the vertical component. An abrupt variation on dominant frequency occurs on all components (it is most clear in the hydrophone); no explanation could be found for this behavior.

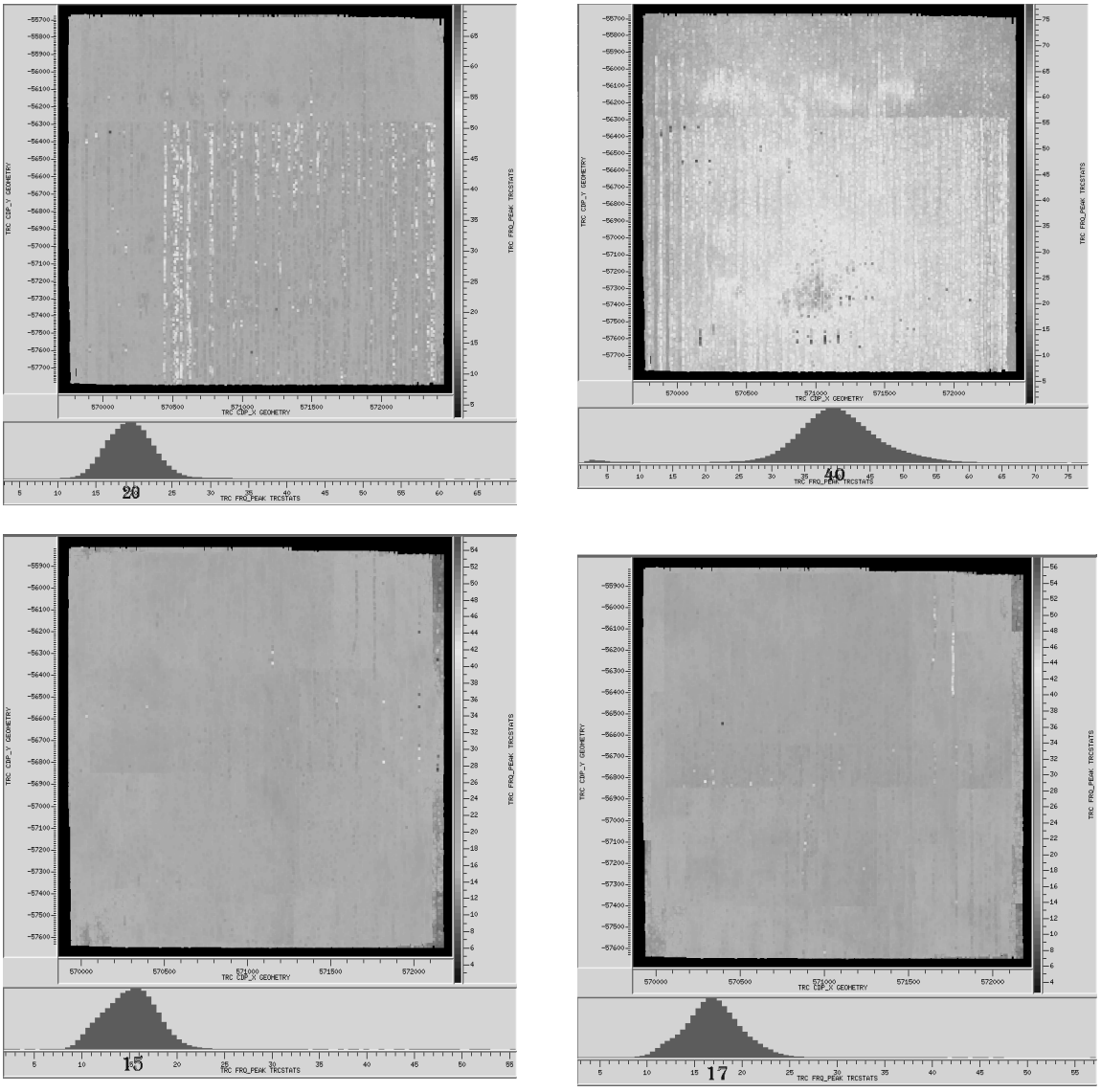

Figure 7 – Average dominant frequency per trace for vertical (top left), hydrophone (top right), radial (bottom left) and transverse (bottom right). No explanation could be found for the sharp variation in the dominant frequency distribution (most clear in the hydrophone).

VERTICAL AND HYDROPHONE COMPONENTS

A spiking deconvolution with 240 ms operator length (also tested were 80, 160 and 320 ms) and 0.1 white noise was applied. An example of a CDP gather for both components is presented on Figure 8. The hydrophone data seems to have better quality, with more continuity in the events and a higher frequency content (although,

as previously said, it can be related to energy reverberation). One interesting aspect in the vertical gather is that some adjacent traces seem very similar to each other. The explanation for this is that these traces are grouped by very close offsets, what can be observed at the top of the picture, where the absolute offset is shown.

The amplitude spectra for these gathers are shown on Figure 9. The hydrophone data have strong notches, at frequencies close to the one expected from the water depth in the area (85 m). The absence of notches in the vertical could be due to presence of shear-wave energy in this component, what is not refused when a radial processing flow is applied on vertical data, as will be shown later in this report.

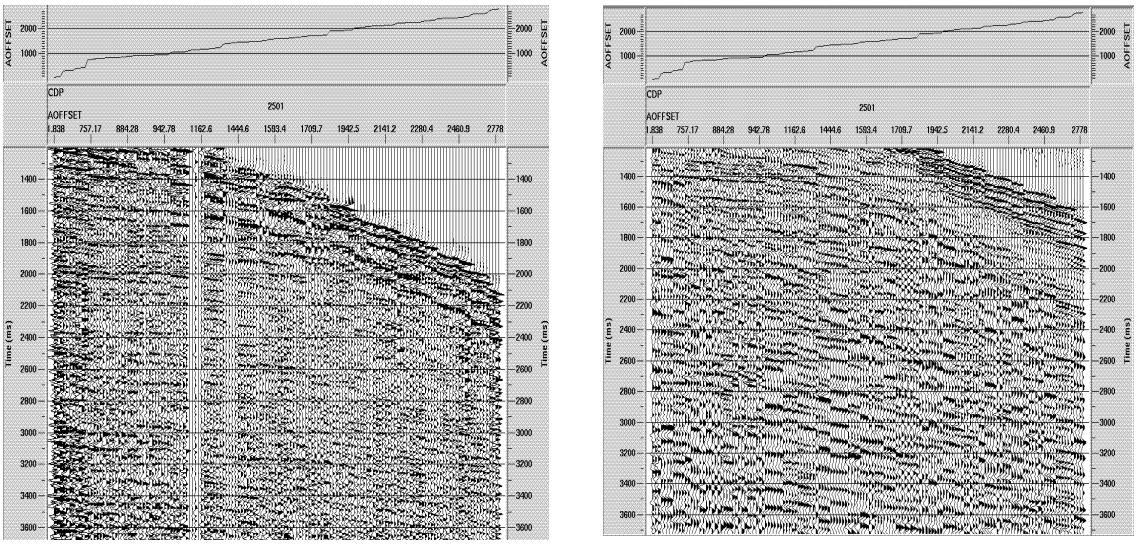

Figure 8 – Example of CDP gather for hydrophone (left) and vertical component.

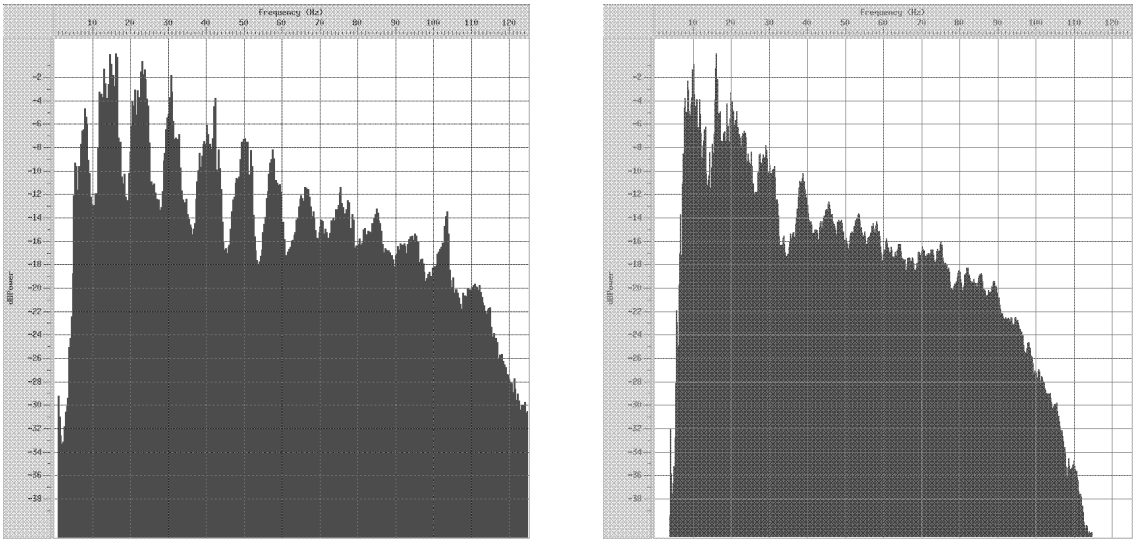

Figure 9 – Amplitude spectra on stacked data for hydrophone (left) and vertical component.

The first receiver statics obtained were by hand. This was done by picking a continuous event (not necessarily flat) on a stacked section sorted by receivers. The

picked event was smoothed, so that its 'regional' (long wavelength) time variation was preserved and the smoothed event subtracted from the original one. This difference was considered to be caused mainly by receiver statics. As some existing geological structure is preserved on this process (which may not be true on refraction statics), this process is called 'structural statics'. This process was run four times for the vertical and three times for the hydrophone.

The source statics were obtained from the vertical component, and considered the same for all other components. Only residual statics were obtained for shots. The statics were obtained by correlation of the analyzed trace (one trace each time) with a 'pilot' trace. The pilot trace came from stacked data (sorted by source), with some random noise attenuation process applied. The static value is considered the shift that gives the best correlation between the analyzed and pilot trace, based on a stack power value. This correlation process was applied three times for the source statics. On each successive run, the maximum value allowed for the shift was decreased, from 30 ms on the first run to 15 ms in the last. No surface-consistent processes were used, as we thought that some static shift differences could be caused by different receiver responses according to the kind of deployment used, and we wanted to preserve them. The results are presented on Figure 10. The statics are small and are grouped around zero, even for the first run. After three runs, very few shots have statics over +/- 15 ms, and the concentration around zero has a remarkable increase when compared to the first run.

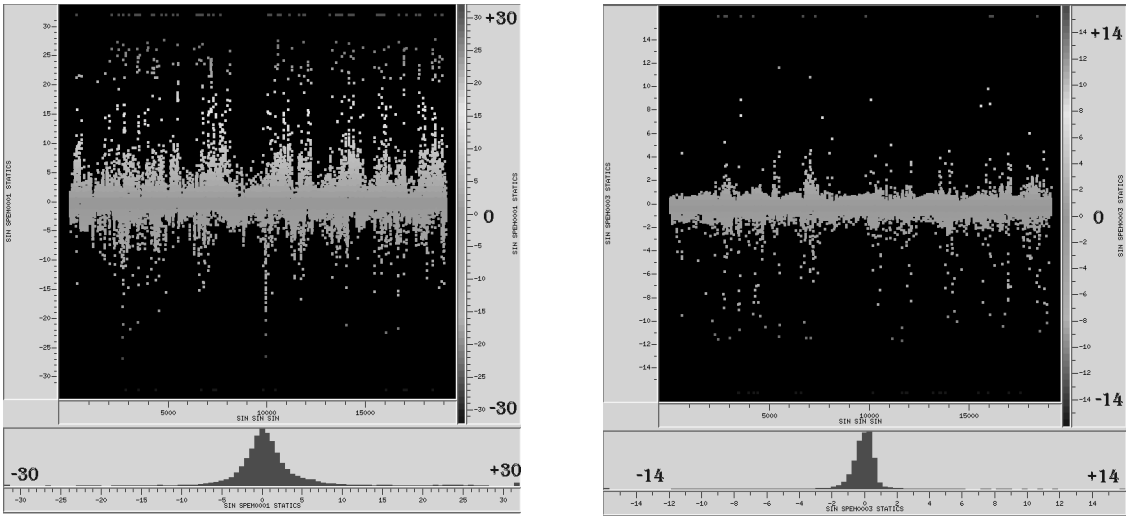

Figure 10 – Static corrections for the source, obtained in the vertical component and applied to all components. First (left) and third (right) run of residual statics by cross-correlation. No hand statics were applied for the shots.

The same process was used to obtain receiver residual and trim statics. Two runs were enough for both vertical and hydrophone. Figure 11 shows an example of hand and residual statics for the hydrophone.

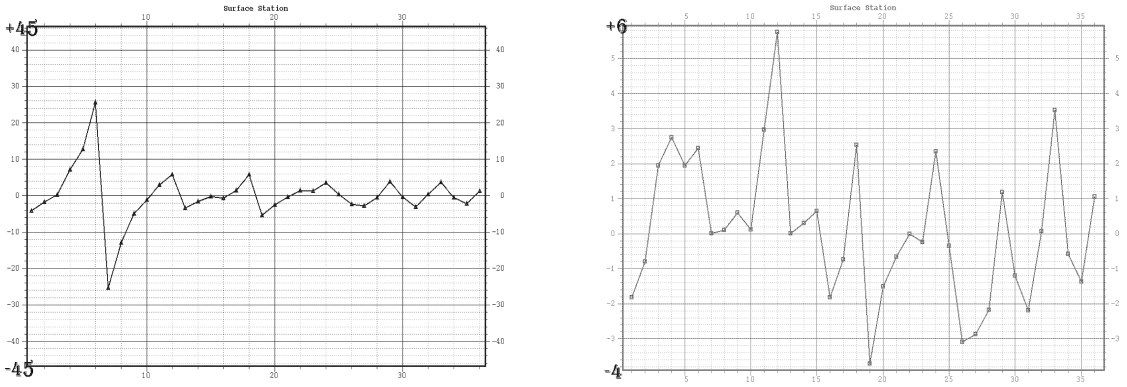

Figure 11 – Static corrections for hydrophone: second run of hand (left) and first residual (right).

After the statics, a new velocity analysis was performed, and the data sorted by CDP and stacked. Cancellation of stretched signal was done using a top mute designed on NMO corrected gathers, not by a constant (e.g. 30 %) value. As previous reports on this area (Ebrom *et al.*, 1998) show the presence of dipping events, it was decided to apply dip move out (DMO) to the data. Figure 12 shows a comparison between stacked hydrophone data with and without DMO. As they look quite similar, and no section is better for all events, which result is better can be decided only by some interpreter familiar with Teal South area. Regarding velocity analysis, though, Figure 13 shows very clear that DMO allows a better velocity picking due to better semblance focusing.

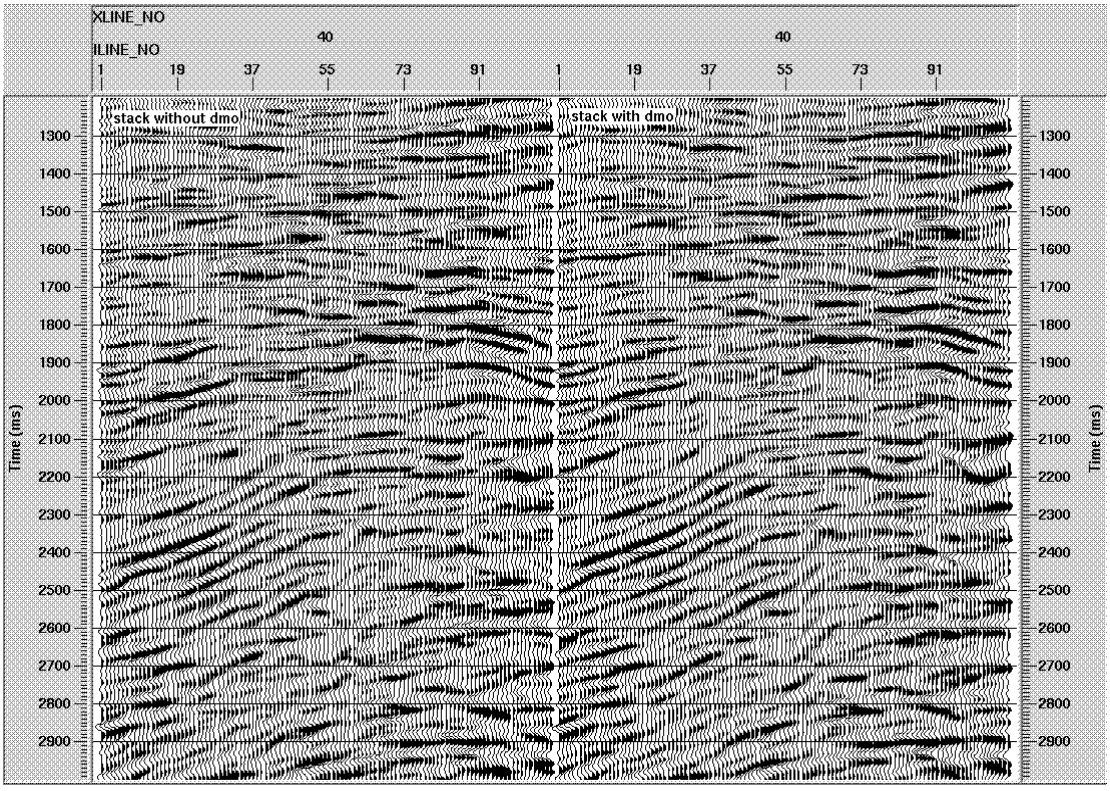

Figure 12 – Comparison on hydrophone stacked data without (left) and with (right) DMO.

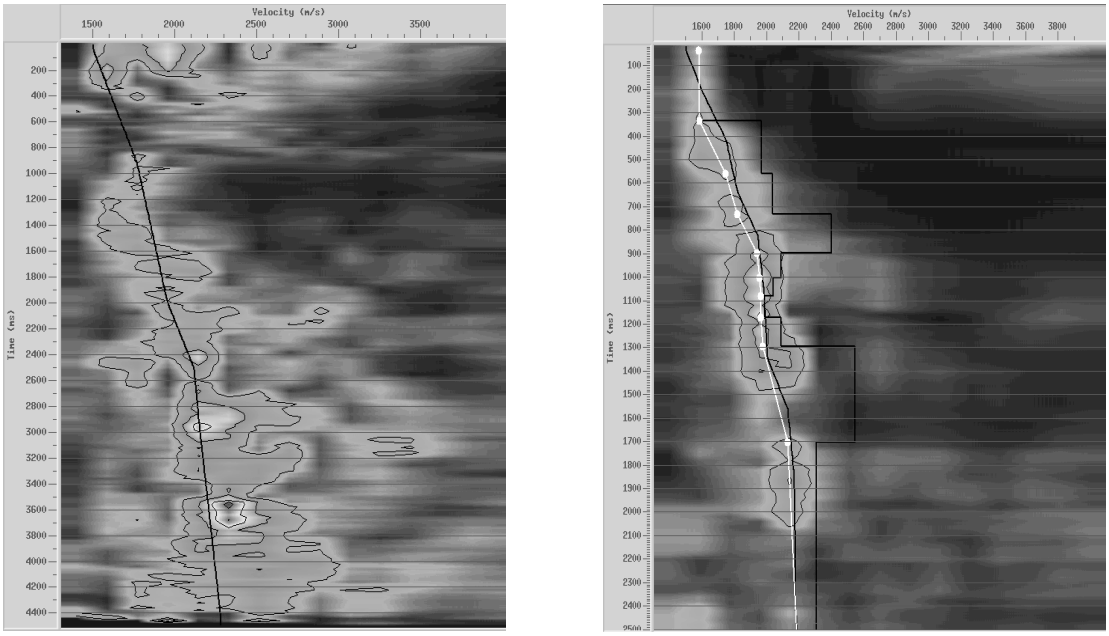

Figure 13 – Velocity analysis after DMO. Black function show velocity picked on data without DMO, white function velocity picked after DMO.

After stack, a finite-difference time migration was applied. The result, for hydrophone data with and without DMO, is shown on Figure 14. Again, the use of DMO makes small differences on the final result.

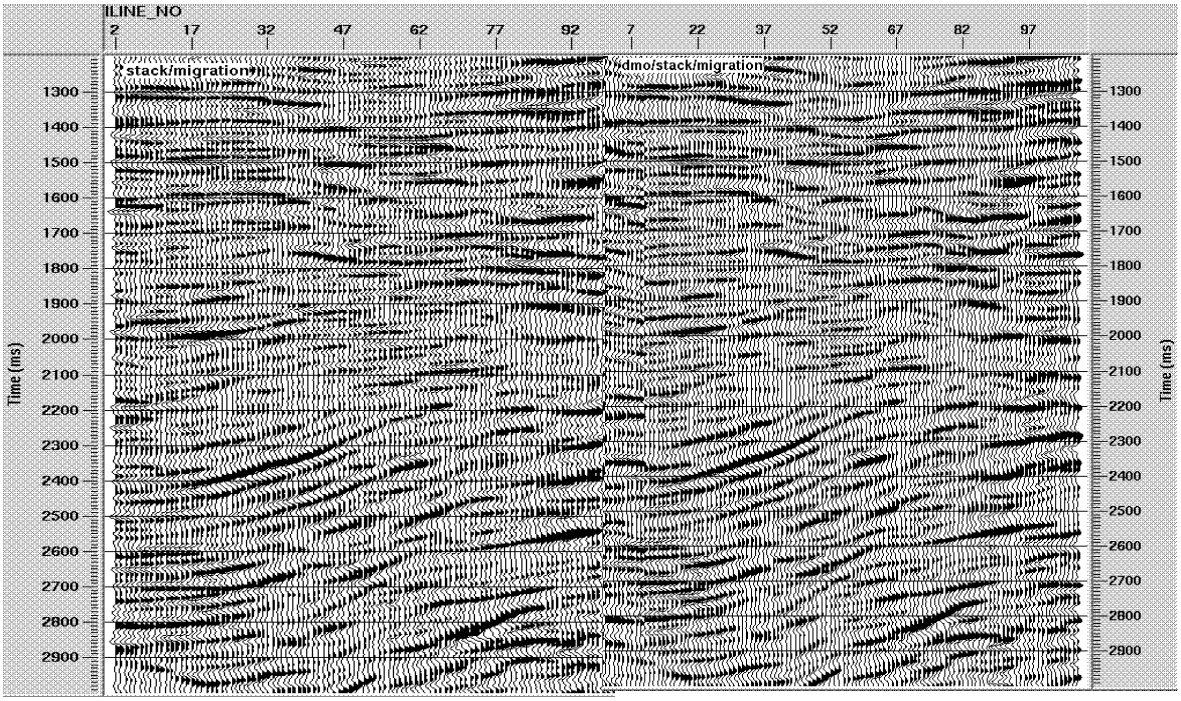

Figure 14 – Comparison of migrated data without (left) and with (right) DMO for hydrophone.

A 3-D pre-stack time migration algorithm, based on the equivalent offset migration, developed in CREWES by John Bancroft and Xinxiang Li, was applied to the hydrophone data. The results, presented on Figure 15, show that EOM method produces a section with lower frequency content and less continuous events. The possible reasons for this are being currently analyzed.

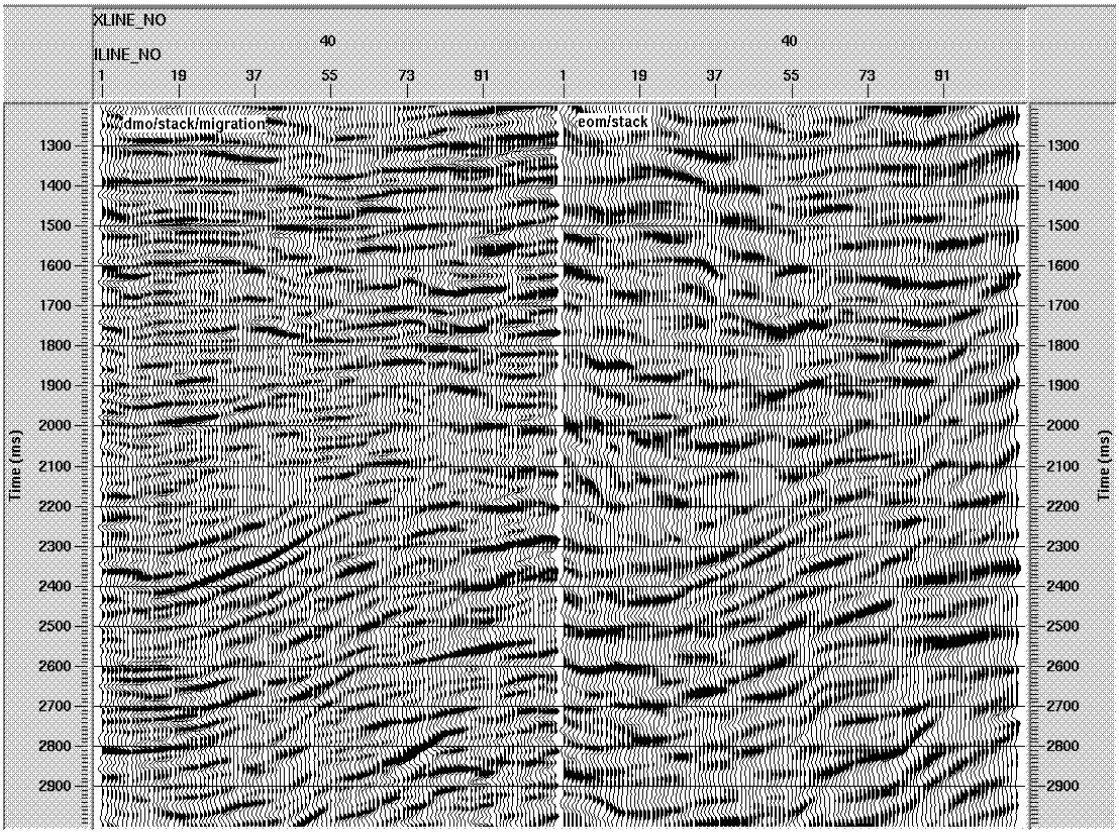

Figure 15 – Comparison between hydrophone data after DMO, stack and post-stack finite difference migrated (left) and after EOM and stack (right). Observe lower frequency and less event continuity on EOM results.

A general processing flow for the vertical and hydrophone components is shown in Figure 16. The final velocity analysis was done on a 250 x 250 m grid.

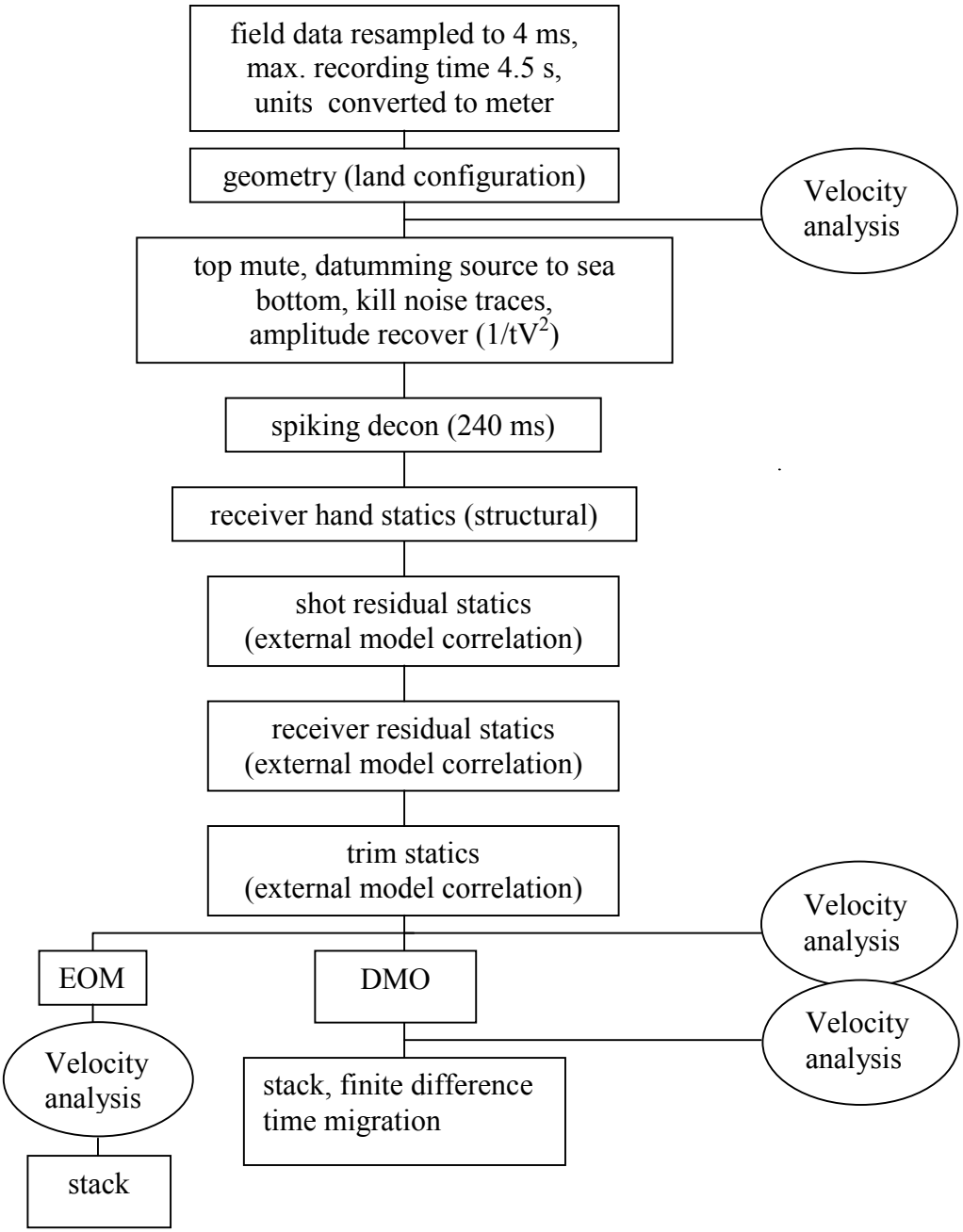

Figure 16 – Processing flow for vertical component and hydrophone. The shot static was obtained only in the vertical flow. In the hydrophone amplitude recovery, a inelastic correction (α=0.002) was also used.

RADIAL AND TRANSVERSE COMPONENTS

After reorientation, a sequence similar to the one applied to vertical and hydrophone was applied to radial and transverse components. The most remarkable difference is the use of asymptotic binning, when the P- to S- conversion point at each interface is approximated by a point located at infinity depth, for a specific source and receiver location and V_P/V_S ratio.

For both radial and transverse components, the amplitude recovery used a $1/tV^2$ equation and inelastic correction (α=0.002). No deconvolution was applied to the horizontal components, as some testing on stacked sections showed best results when no decon was used.

Figure 17 shows a radial CCP gather after asymptotic binning, without receiver statics. The data has a regular quality. As for the vertical, some groups of traces look similar due to its close spatial location. Also shown is the amplitude spectrum of this gather. As expected, the frequency content is much lower than vertical component (compare with Figure 9), and a strong drop from –10 to –30 dB occurs around 30 Hz.

Figure 18 present hand (structural) and residual receiver statics for radial component. As expected, hand statics are much higher (sometimes more than twice) in the radial component than hydrophone statics (compare with Figure 11). The picture also shows that after three interactions the residual statics becomes negligible.

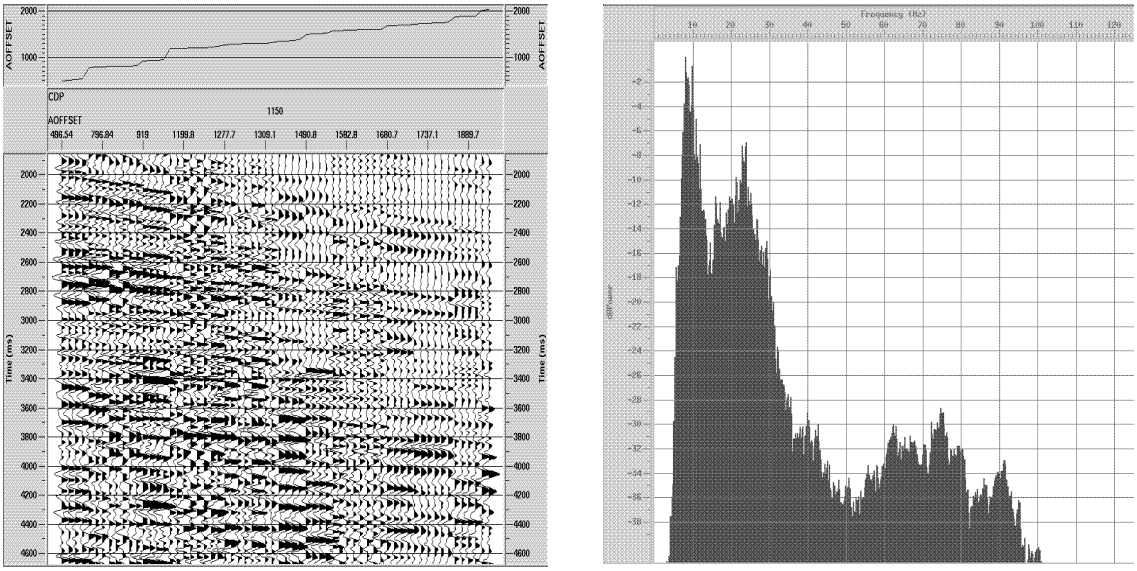

Figure 17 – Radial component CCP gather after horizontal reorientation and asymptotic binning (V_P/V_S=2.0) and its amplitude spectrum.

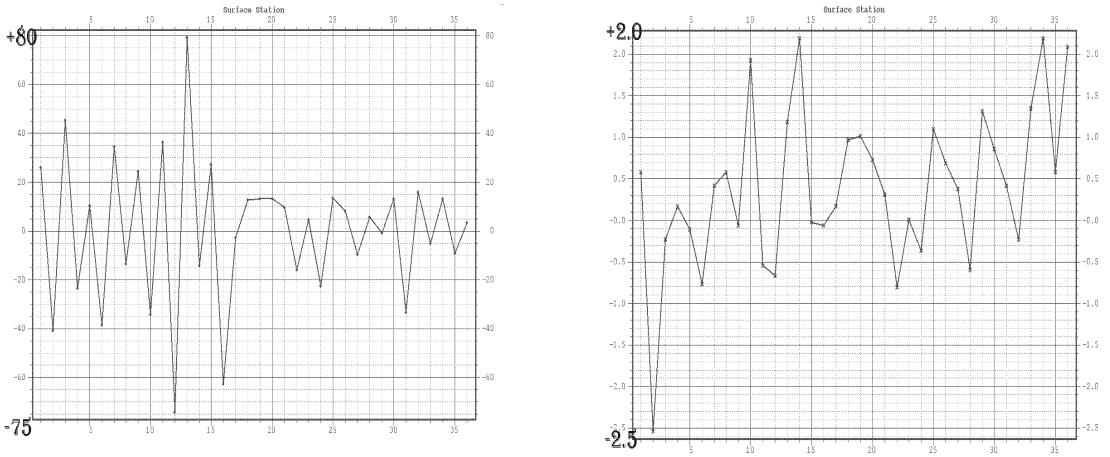

Figure 18 – Hand (left) and residual radial (right) receiver statics, both after three runs.

After all statics were obtained, a new velocity analysis was performed and the data stacked. Converted-wave DMO was applied on both horizontal components. The result for radial is shown in Figure 19. In general, DMO seems to decrease data quality, generating coherent linear noise (mainly in the shallow part of the section). For some events, though, it seems to increase continuity – again, the final opinion has to be given by an interpreter of the area.

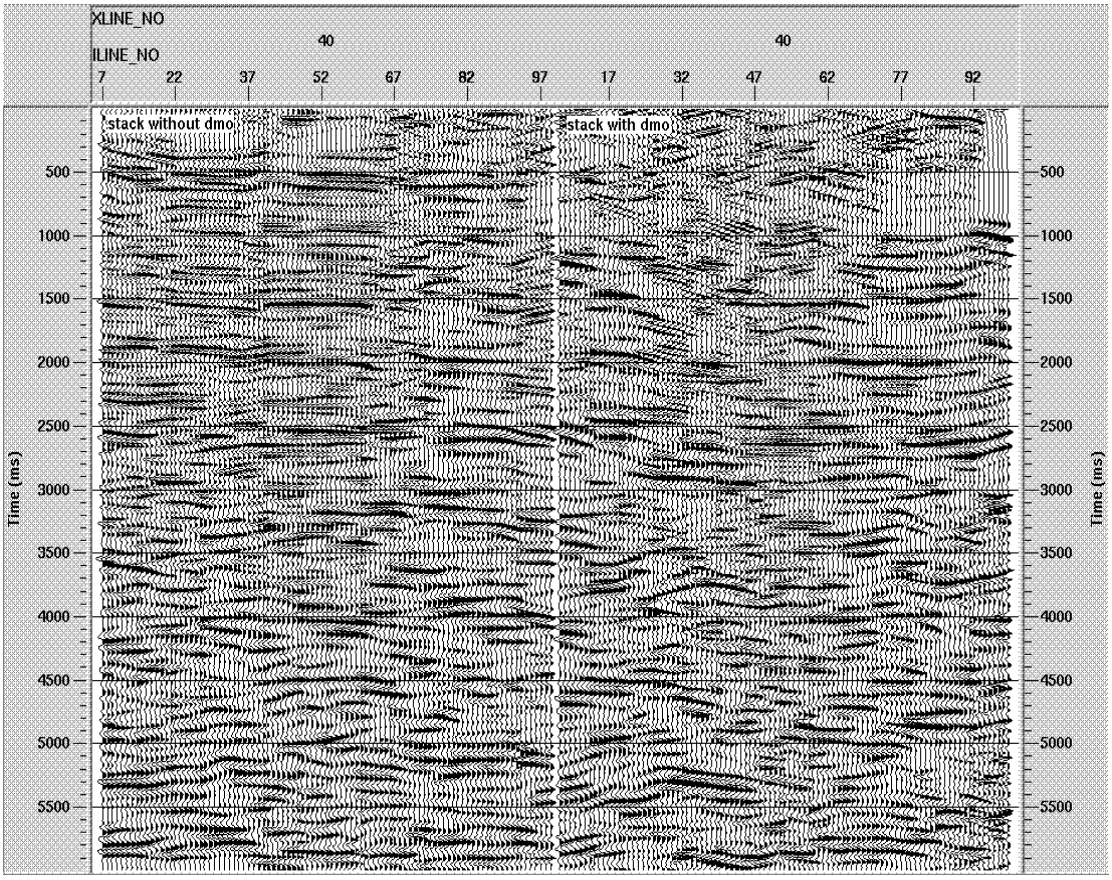

Figure 19 – Comparison between stacked radial data without (left) and with (right) converted-wave DMO.

Another test done in the radial component was the depth-variant stack. This process tries to consider the actual conversion point for different depths. For this, it uses a time and spatial variant V_P/V_S ratio. The results (Figure 20) show this process did not work well, as the conventional stack presents a better section.

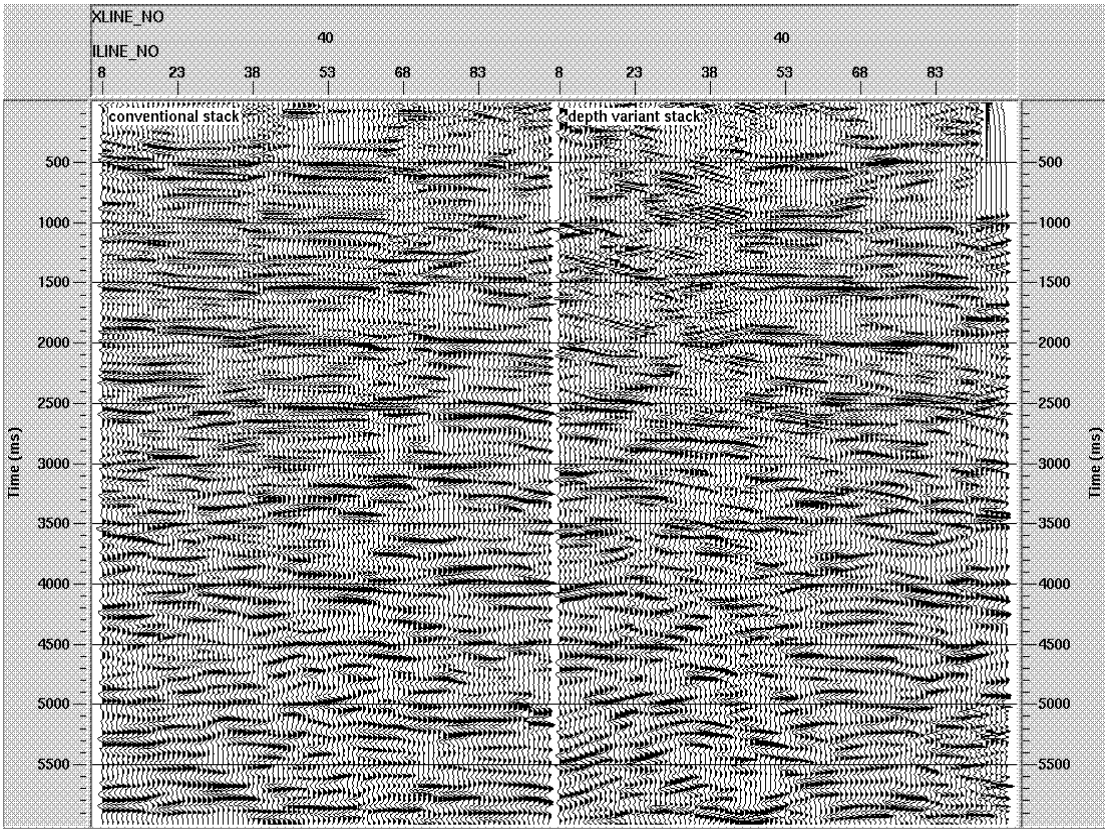

Figure 20 – Comparison between conventional (left) and depth variant stack (right).

The use of effective interval V_P/V_S ratio to theoretically account for transversely isotropic media, which affects the location of the P- to S- conversion point in depth as well laterally, was tested in the radial component. Figure 21 shows the results, which are not good, mainly in the shallow part. This may be due to the use of poor interval V_P/V_S ratios and/or the fact that this process does not allow spatial variation of V_P/V_S ratios.

Also used in the radial data was the equivalent offset migration (EOM) method. The result (Figure 22), except for the shallow part, can be considered better than conventional stack and post-stack migration. The decrease in high frequency content also occurs here, but is not dramatic as in the hydrophone case (compare with Figure 15). Unlike the hydrophone data, though, there is more continuity in the reflection. The algorithm used is suitable for use only after asymptotic binning, so it uses only an approximation of the conversion point, as it consider the scatter point to be positioned in half source-receiver offset. Regardless of this approximation, we do consider it gives better result than conventional processing sequence.

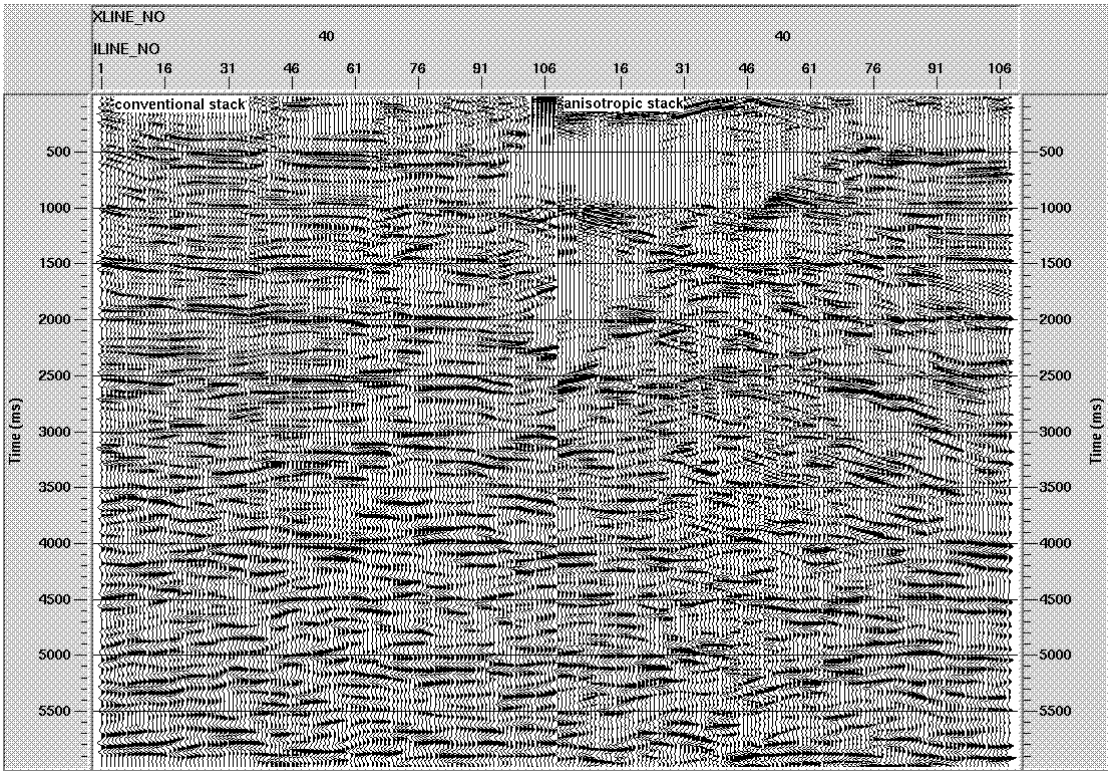

Figure 21 – Comparison between conventional (left) and anisotropic stack (right).

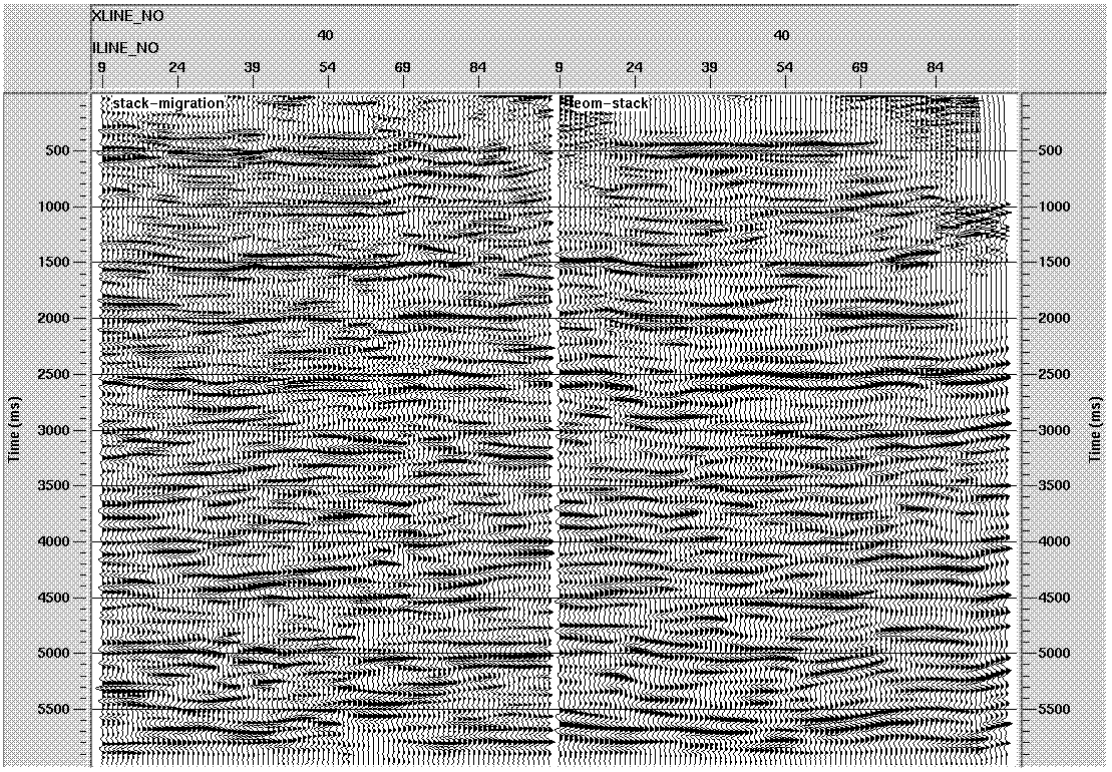

Figure 22 – Comparison between post-stack finite difference migration (left) and EOM followed by stack (right).

Figure 23 shows the processing flow applied in the horizontal components.

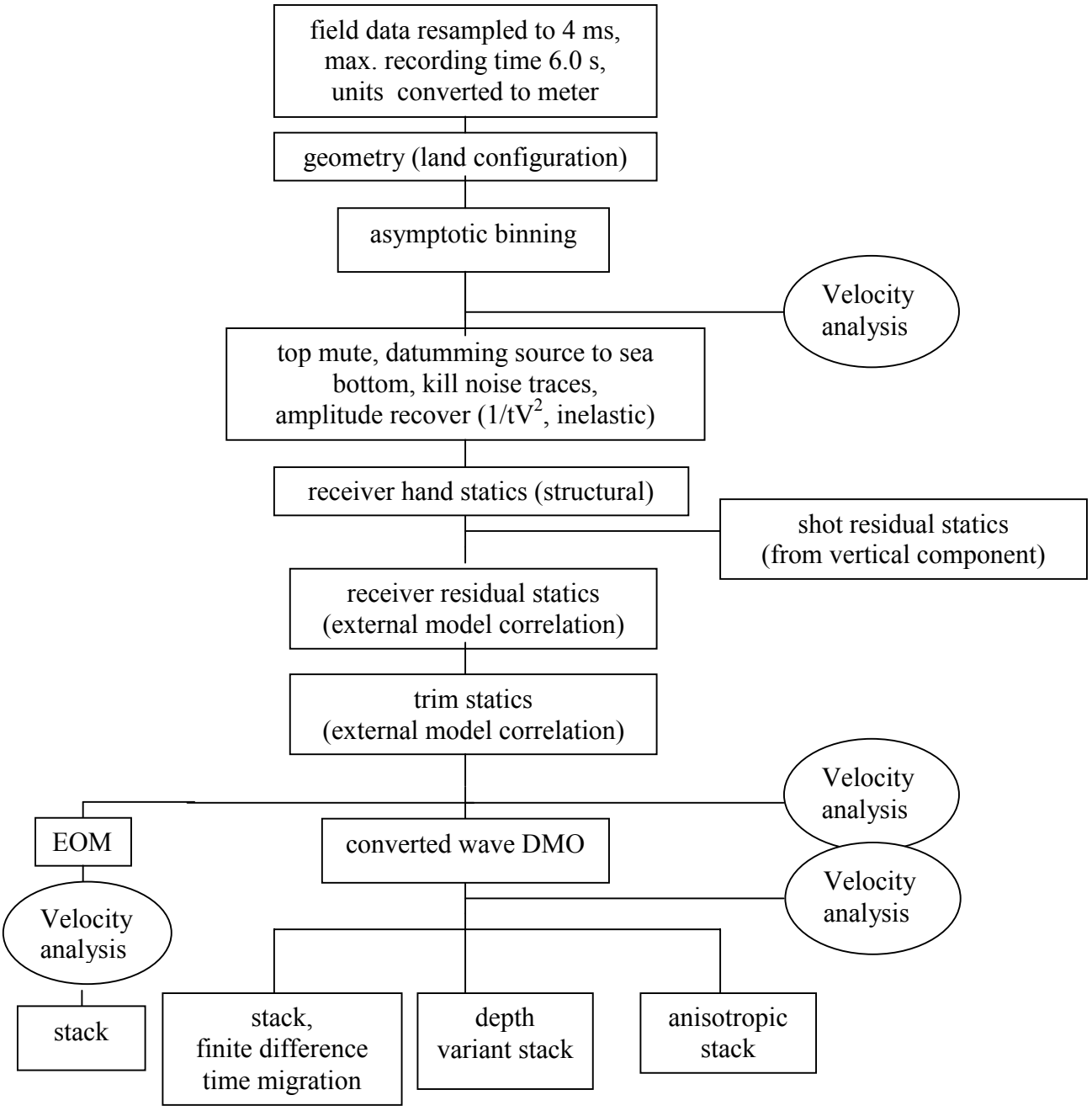

Figure 23 – Processing flow for radial and transverse components.

Future work for the radial component is related mainly to use of different (higher) V_P/V_S for asymptotic binning; values of 2.5 and (depending on the result of 2.5) 3.0 may be tested.

COMPARISON OF CABLE DEPLOYMENT TECHNIQUES

As pointed out in the introduction sections, one purpose of the Teal South project is to analyze which – if any – ocean cable deployment method is superior. We compare the three ways – trenched, taped and taped and sandbagged –, considering all differences among stacked data collected in each cable being caused only by the way it was deployed. In other words, we consider that, mainly due to the small distance (around 100 m) between the analyzed cables, geological changes were not important. The cables to be compared are the ones in the N-S direction, located in easternmost part of the survey. The same processing parameters (statics, velocities, etc) were used for all cables, and the hydrophone and radial components were used in the analysis.

Figure 24 shows a comparison between the trenched cable versus the cable laid on sea bottom with taped receivers. We found the taped cable to have better quality than the trenched one, mainly in the radial component. However, a final opinion can be given only by someone familiar with the geology of the area, as the differences are not dramatic.

When data from the trenched cable is compared with data from the cable laid on the sea bottom with receivers taped and sandbagged (Figure 25), we find that, for most events, there is more continuity in the taped and sandbagged case. This is true for both components.

Figure 26 shows the final comparison, when both cables are laid on the sea bottom and have the receivers taped, but in one cable, sandbags are also put over the receivers. In our opinion, the use of sandbags deteriorates data quality for both components. One could expect the opposite (sandbagged receivers should give better data), as they should have, at least theoretically a better coupling and less ambient noise susceptibility. Some hypotheses are: 1) the sandbags generate some kind of noise when seismic waves propagate trough it, and/or 2) the receivers (both geophone and hydrophone) decrease their performance if some weight is put directly over them.

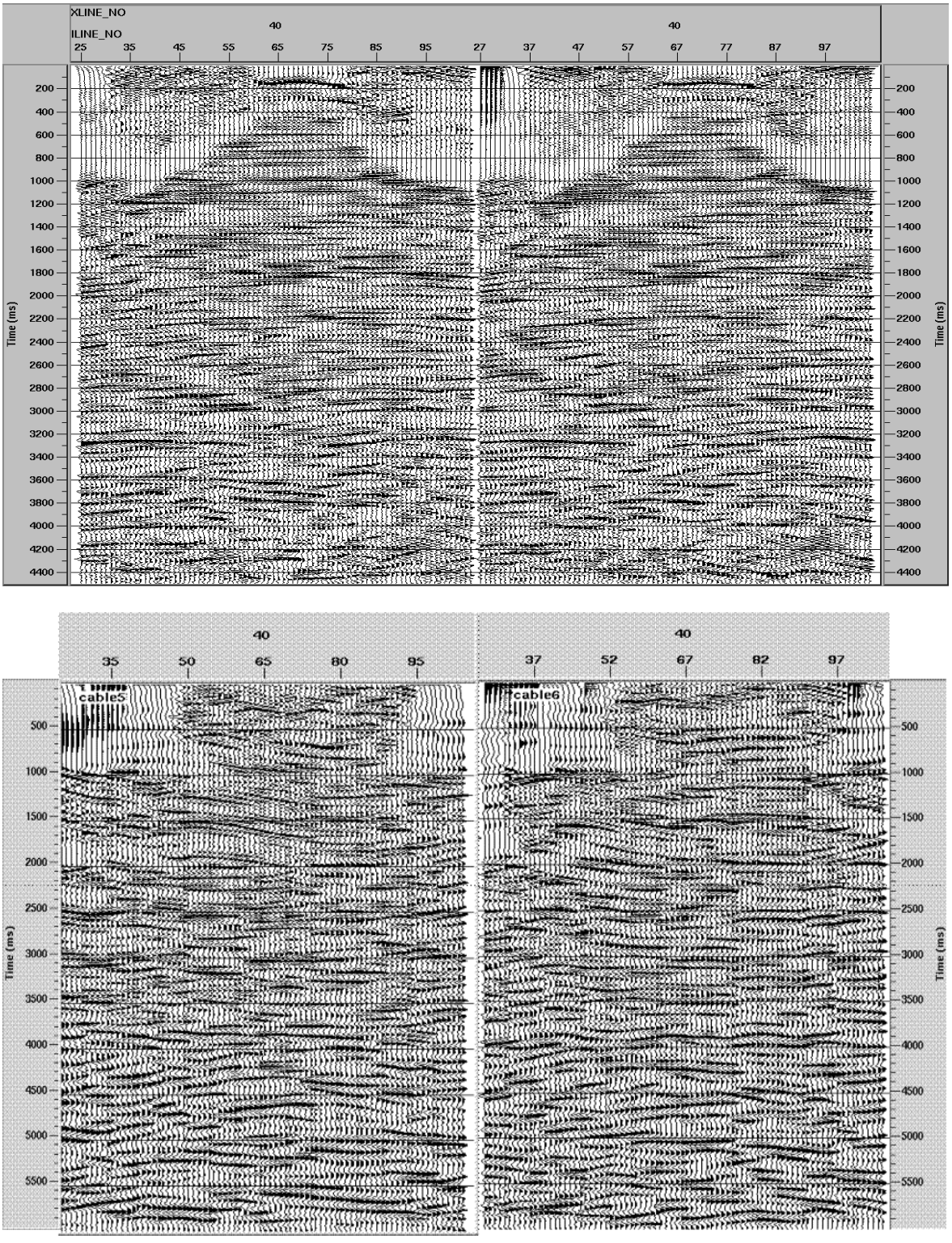

Figure 24 – Comparison between data collected from cable trenched (left) and taped (right). Hydrophone at top and radial at bottom.

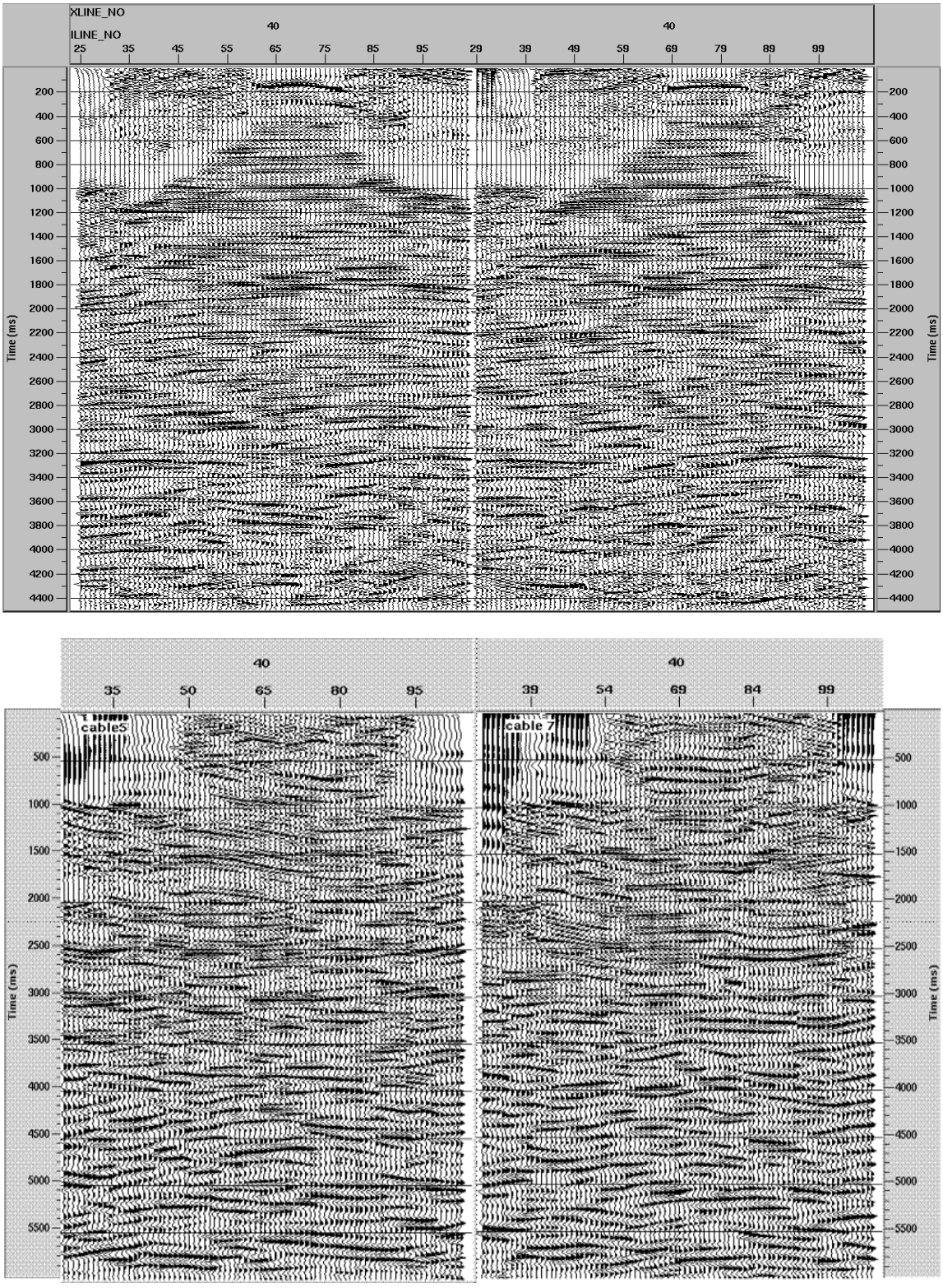

Figure 25 – Comparison between data collected from cable trenched (left) and taped and sandbagged (right). Hydrophone at top and radial at bottom.

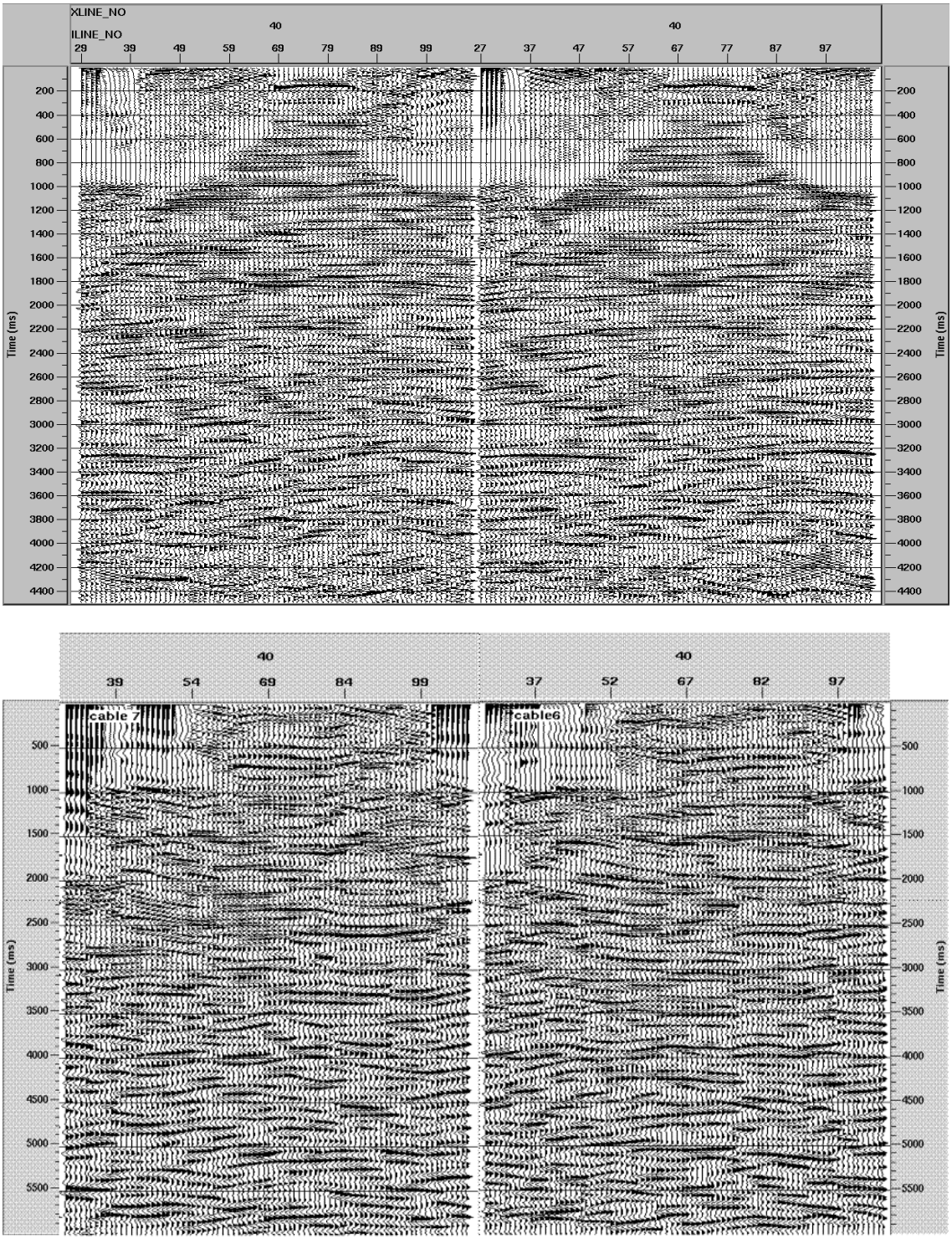

Figure 26 – Comparison between data collected from cable taped and sandbagged (left) and taped (right). Hydrophone at top and radial at bottom.

P-S ENERGY ON VERTICAL COMPONENT, P-P ON RADIAL

To verify the presence of compressional wave energy in the radial component, the vertical processing flow – shown in Figure 16 – and its parameters (including statics and velocities functions) were applied in the data from the radial component after reorientation. From the result, presented in Figure 27, we see that almost no coherent events are obtained. It can be concluded that very little P-P energy is present in the radial component, probably because the compressional energy is arriving at sea bottom close to the vertical.

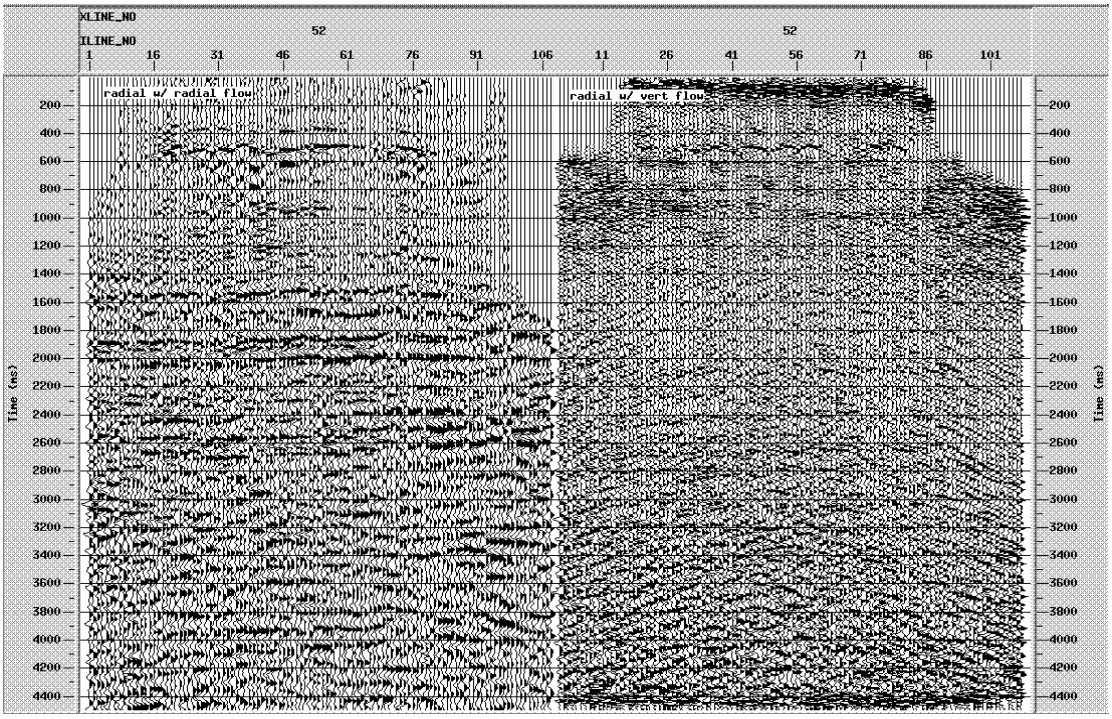

Figure 27 – Comparison between radial data processed with 'conventional' flow (shown in Figure 23), at left, and the same data processed with vertical component flow (shown in Figure 16), at right.

On the same way, the presence of shear wave energy in the vertical component was verified applying the radial component flow (shown in Figure 23) in the vertical component data. One can see (Figure 28) that many events are present, showing that the vertical data as processed here may be highly contaminated with converted-wave (P-S) energy.

The separation of these energy modes in the appropriate components is considered as future work.

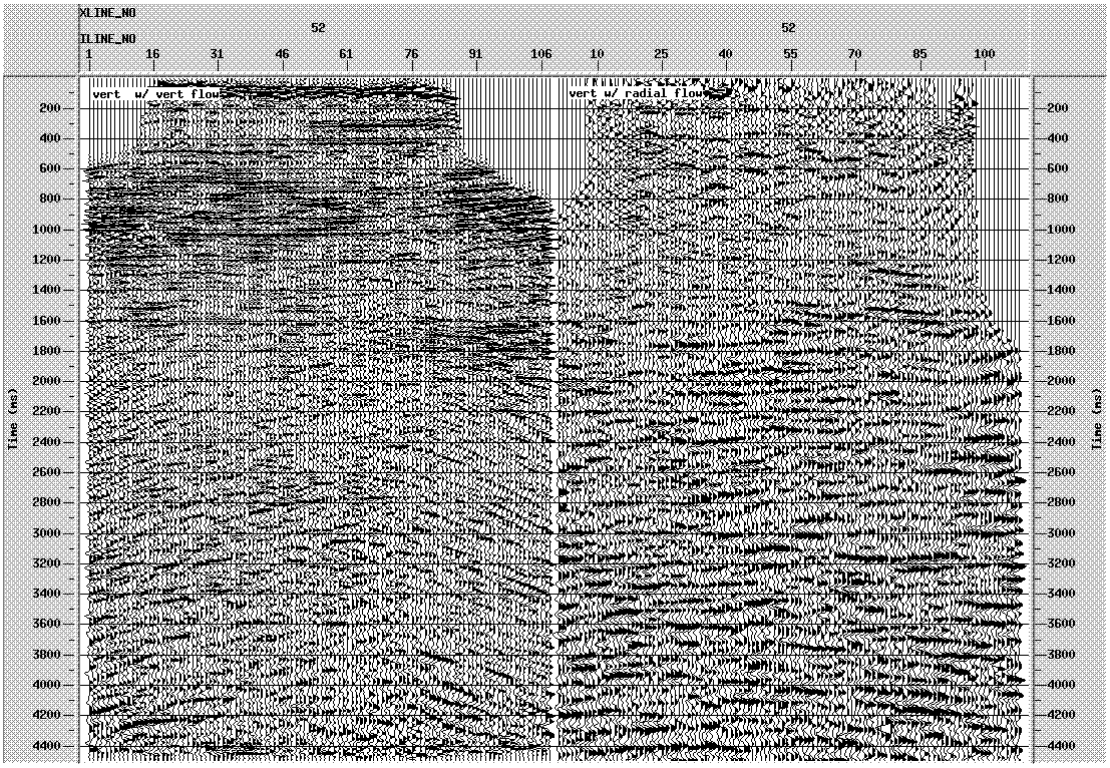

Figure 28 – Comparison between vertical data processed with 'conventional' flow (shown in Figure 16), at left, and the same data processed with radial component flow (shown in Figure 23), at right.

CONCLUSIONS

Conventional and CREWES specific flows were applied to the data. The best quality was present on the hydrophone, followed by the vertical and then the radial. 3-D pre-stack time migration generated low frequency data on vertical and hydrophone but better quality on radial.

From the three methods used on cable deployment, best results were found with cable laid on the sea bottom and receivers taped to it. No compressional wave energy was found in the radial component, but the vertical component is contaminated with converted wave energy. Separation of these modes into their components and use of different V_P/V_S ratios for asymptotic binning are the future work priority.

ACKNOWLEDGEMENTS

We thank Xinxiang Li for his patient and continuos discussion on processing of multicomponent seismic data and Brian Hoffe and Roger Entralgo (from ERCH) for their information about Teal South. Appreciation also to Henry Bland for his constant system help.

REFERENCES

Baker Hughes/Western Geophysical, 1999, Energy Research Clearing House, Teal South Phase II 4D/4C, Eugene Island Block 354, Gulf of Mexico, South Louisiana, USA, Spring 1999, Job Number 060-99-001, Final Report.

Ebrom, D., Krail, P., Ridyard, D. and Scott, L., 1998, 4-C/4-D at Teal South: The Leading Edge, 17, no. 10, 1450-1453.

Purnell, G.W., Nolte, B.J., Krail, P.M. and Ebrom, D.A., 1999, Analysis of 4-C data for AVO effects at Teal South, Eugene Island 354. *Offshore Technology Conference 1999*, paper OTC 10984.

Roche, S., Maxwell, P. and Fisseler, G., 1999, Teal South 4C/3D survey: a model for 4C/4D seismic data acquisition. *Offshore Technology Conference 1999*, paper OTC 10983.

Appendix I – Survey Parameters

Source: 2 sub arrays of 750 in^3 each, 3,000 +/- 100 psi, depth 3.0 +/- 0.5 m, acoustic output 39.0 bar-m peak-to-peak (3-128 Hz).

Receivers: 4-C receivers in 7 ocean-bottom cables.

Recording: 24 bits remote recording boxes, 2 ms sampling interval, record length 6 seconds, low-cut filter out (3 Hz 12dB/octave), high cut 200 Hz.

Navigation: DGPS; source tracking by GPS antenna on each gun string, receiver location to be compute using first break.